Multipole strength in ^{12}C from the $(e, e'\alpha)$ reaction for momentum transfers up to 0.61 fm^{-1}

D. J. DeAngelis,* J. R. Calarco, and J. E. Wise†
Department of Physics, University of New Hampshire, Durham, New Hampshire 03824

H. J. Emrich, R. Neuhausen, and H. Weyand
Institut für Kernphysik, Universität Mainz, D-55099 Mainz, Federal Republic of Germany
(Received 24 February 1994; revised manuscript received 30 March 1995)

We have excited the giant resonance region in ^{12}C via inelastic electron scattering, and have measured the first complete angular correlations for charged particle emission for this reaction for four values of momentum transfer ranging from 0.24 fm^{-1} to 0.61 fm^{-1}. By analyzing the α-emission channels via the Legendre and resonance formalisms, we unambiguously determined the multipole contributions to the total cross section for α emission to the ground state of ^{8}Be, and have set limits on these contributions for α emission to the first excited state of ^{8}Be. We have found that, in both cases, $E2$ radiation is the strongest contribution but that $E0$ and $E3$ contributions cannot be ignored. By constructing total multipole form factors and fitting them within the distorted wave Born approximation using a transition charge density specified by the Tassie model, we deduced multipole transition strengths and fractions of the appropriate sum rules. Our results are compared with those from the $(p, p'\alpha)$ and $(\alpha, \alpha'\alpha)$ reactions.

PACS number(s): 24.30.Cz, 25.30.Dh, 25.30.Fj, 27.20.+n

I. INTRODUCTION

While the systematic characteristics of many giant resonance modes are well known in medium and heavy nuclei, the data for light nuclei, which are more amenable to microscopic calculations, are incomplete and inconsistent. In particular, the giant quadrupole resonance (GQR) in ^{12}C has been the subject of a number of studies using various reactions [1–9], which have claimed differing amounts of strength. Electromagnetic probes [1–4] are unique in that they are equally sensitive to both isovector and isoscalar excitations and can, in principle, excite all multipoles. In contrast, hadron scattering is more strongly selective for isoscalar excitations because of the relative weakness of the $t\tau$ component of the hadron-nucleus interaction as evidenced by previous studies using (^{3}He,^{3}He$'$) scattering [5] and (p, p') reactions [6]. Inelastic (α, α') scattering [7] is even more selective due to the $S = 0, T = 0$ nature of the probe.

Since GR's exist in the continuum, a complete description can be achieved only with coincidence measurements. In this case, one can measure angular correlations, which are characteristic of the multipolarity, and choose an emission particle which selects a specific resonance mode. In particular, choosing the α-emission channels provided us with a tool by which, apart from isospin mixing, the isoscalar modes can be studied. Indeed, it has been theoretically shown [10] that for nuclei with $1p$ and $2s$-$1d$ valence orbitals, α emission accounts for most of the GQ$_0$R decay.

In this experiment, we measured the first complete angular correlations for the ^{12}C$(e, e'\alpha)$ reaction for momentum transfers up to 0.61 fm^{-1}. We have performed a multipole decomposition of the cross sections, constructed total multipole form factors from this decomposition, and extracted multipole transition strengths and sum rule fractions. We found that the dominant multipole is $E2$ [11] but that $E0$ and $E3$ contributions cannot be ignored.

II. THEORETICAL CONSIDERATIONS

In the plane-wave Born approximation, the general form of the electron scattering cross section is typically expressed as [12]

$$\frac{d^5\sigma}{d\Omega_e d\Omega_x d\omega} = \sigma_M (V_L W_L + V_T W_T + V_{LT} W_{LT} \cos\varphi_x + V_{TT} W_{TT} \cos 2\varphi_x) \ . \quad (1)$$

The kinematic dependence of Eq. (1), given in terms of the four-momentum transfer Q, the three-momentum transfer q, and the electron scattering angle ϑ_e, is expressed through the V's

$$V_L = \left(\frac{Q}{q}\right)^4 , \quad (2)$$

$$V_T = \frac{1}{2}\left(\frac{Q}{q}\right)^2 + \tan^2\left(\frac{\vartheta_e}{2}\right) , \quad (3)$$

*Present address: Department of Radiation Oncology, University Hospital, Stony Brook, NY 11794.
†Present address: Department of Physics, Northwestern University, Evanston, IL 60208.

$$V_{LT} = \left(\frac{Q}{q}\right)^2 \left[\left(\frac{Q}{q}\right)^2 + \tan^2\left(\frac{\vartheta_e}{2}\right)\right]^{1/2} , \quad (4)$$

$$V_{TT} = \frac{1}{2}\left(\frac{Q}{q}\right)^2 , \quad (5)$$

where the energy transfer ω relates Q and q, $Q^2 = q^2 - \omega^2$. The Mott cross section for scattering off a point charge is given by

$$\sigma_M = \left(\frac{\alpha\hbar c \cos(\vartheta_e/2)}{2E_i \sin^2(\vartheta_e/2)}\right)^2 , \quad (6)$$

where E_i is the incident electron energy, while the W's reflect the nuclear dynamics. The subscripts L and T refer to interaction of the exchanged virtual photon with the longitudinal and transverse nuclear currents, while the subscripts LT and TT refer to longitudinal-transverse and transverse-transverse interferences, respectively. Figure 1 illustrates the kinematics and the coordinate system used to define the particle emission angles. Here, the polar angles of the emitted particle, ϑ_x, is defined with respect to $\mathbf{q}$, and ϕ_x, the azimuthal (out-of-plane) angle of the emitted particle, is defined with respect to the electron scattering plane as in, for example, de Forest [12].

If the cross section is dominated by a few multipoles, as it is in the resonance region, then it is useful to expand Eq. (1) in terms of Legendre polynomials [13]

$$\frac{d^5\sigma}{d\Omega_e d\Omega_x d\omega} = \sigma_M \sum_{l=0}^{2} \sum_{k=l}^{2L} A_k^l P_k^l(\cos\vartheta_x)\cos(l\varphi_x) , \quad (7)$$

where the response functions W_L and W_T both contribute to the A_k^0 coefficients, and the A_k^1 coefficients constitute a multipole decomposition of the 3rd response function, W_{LT}. By fixing the out-of-plane angle at 135°, W_{TT} and its expansion in A_k^2's was eliminated from the sum. This removes any ambiguity in the analysis since the P_k^2's are not independent of the P_k's.

In the approximation that the reaction cross section is resonance dominated, the Legendre coefficients can be factored into excitation form factors, which depend only on the nuclear dynamics and q, and angular correlation shape coefficients which depend only on the particle emission and ω and are independent of q [13–15]. Following the static limit resonance approximation (SLRA) of Kleppinger and Walecka [13], the longitudinal and transverse excitation form factors are given by $C(L)$ and $T(L)$, respectively, while the shape coefficients are given by $a_k(L)$ and $a_k(L, L')$ for pure and interfering radiation, respectively.

If, for example, the cross section is entirely $E2$ in nature, then the pertinent Legendre coefficients can be written within this approximation as

$$A_0^0 = V_L|C(2)|^2 + V_T|T(2)|^2 , \quad (8)$$

$$A_2^0 = a_2(2)(2V_L|C(2)|^2 + V_T|T(2)|^2) , \quad (9)$$

$$A_4^0 = a_4(2)\left(-\frac{3}{2}V_L|C(2)|^2 + V_T|T(2)|^2\right) , \quad (10)$$

$$A_2^1 = \sqrt{\frac{2}{3}}a_2(2)(V_{LT}|C(2)||T(2)|) , \quad (11)$$

$$A_4^1 = -\frac{3}{4}\sqrt{\frac{2}{3}}a_4(2)(V_{LT}|C(2)||T(2)|) , \quad (12)$$

where $4\pi A_0^0$ is the total $E2$ cross section. Further, if the α emission populates the 0^+ ground state of the residual nucleus ^{8}Be (α_0 emission), then there is only one partial wave which contributes to the outgoing α wave function and the shape coefficients are uniquely determined from angular momentum coupling considerations. This is not the case for α emission to the first excited state of ^{8}Be (α_1 emission) at 2.93 MeV. Full expressions for the cross section derived within the SLRA for multipoles up to $L = 3$, as well as interferences between these multipoles, are given in the Appendix.

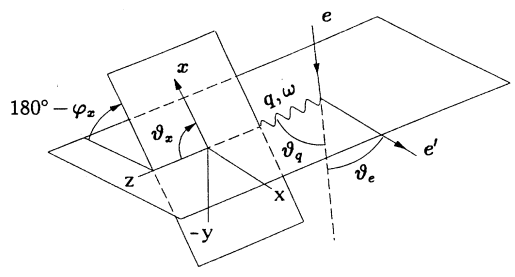

FIG. 1. Kinematics for ^{12}C$(e, e'x)$. The particle emission plane, indicated by the right-handed coordinate system, was fixed at an azimuthal angle of $\varphi_x = 135°$.

III. EXPERIMENTAL CONSIDERATIONS

Data for the reactions ^{12}C$(e, e'x)$, where $x = p, \alpha$, were accumulated at the Institut für Kernphysik, Universität Mainz using the microtron MAMI-A [16]. Continuous wave electron beams of 124.1 and 183.4 MeV, with average currents between 8–15 μA, impinged on self-supporting carbon foils of natural isotopic composition with thicknesses of 2.4 and 3.6 mg/cm^2. The scattered electrons were detected in the 180° double-focusing magnetic spectrometer [17], the focal plane of which was fitted with an array of overlapping scintillators and Čherenkov counters. The spectrometer was set between 22° and 40° defining momentum transfers of 0.24, 0.35, 0.41, and 0.61 fm^{-1}, and had a solid angle of 4.0 msr, a momentum acceptance of 6%, and a momentum resolution of 2.5×10^{-4}. The measured excitation energy range was ω = 18–28 MeV. For all data runs, the electron arm resolution was significantly better than the smallest $\Delta\omega$ bin size for α emission used in our analysis.

TABLE I. Specifications for the Mainz detectors and telescopes. The detector thickness and area and telescope solid angle and stopping power are given by t, A, Ω_x, and S. The labels "ΔE," "E," and "$\Delta E + E$" refer to the first detector, the second detector, and both detectors, while "p" and "α" refer to protons and alpha particles.

$t(\Delta E)$		75 μm
$t(E)$		1000 μm
$A(\Delta E)$		300 mm^2
$A(E)$		450 mm^2
Ω_x		22.4, 39.4 msr
$S(\Delta E)$	p	2.7 MeV
	α	10.8 MeV
$S(\Delta E + E)$	p	12.8 MeV
	α	51.3 MeV

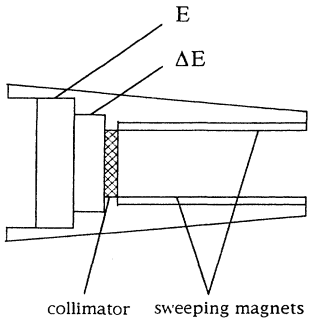

FIG. 3. A telescope cross section. ΔE and E indicate 75 μm and 1000 μm silicon surface barrier detectors. The collimator defined the telescope solid angle and the sweeping magnets eliminated low-energy Møller electrons.

The charged particle emission products were detected in coincidence with the scattered electrons by transmission-mount silicon surface-barrier (SSB) detectors arranged in ΔE-E telescopic arrays. These telescopes were mounted on a goniometer—a ring that could be rotated out of the electron scattering plane about $\mathbf{q}$ and rotated in its own plane—such that angular correlations could be measured. Since the goniometer was always fixed at an out-of-plane angle $\varphi_x = 135°$ as shown in Fig. 1, we had complete freedom to vary ϑ_x in the particle emission plane without interfering with the incident or scattered electrons. This allowed for the first complete angular correlation measurements for these reactions.

In order to eliminate low-energy Møller electrons, permanent magnets were placed in front of the telescopes. Specifically, SmCo magnets were employed which created a field of about 0.1 T over a distance of 2 cm. This field effectively swept away electrons of up to 1 MeV thus allowing for cleaner data.

For all of the data runs, the SSB detectors were arranged into seven telescopes with two detectors per telescope. The specifications for these detectors and telescopes are given in Table I. The detector thicknesses were chosen based on the maximum proton kinetic energy of interest and were more than adequate to stop all α particles. The decay α's were detected for $E_\alpha \geq 2.5$ MeV.

For each momentum transfer point, the seven telescopes were configured in two different ways and the goniometer was set to four distinct positions: two aligned roughly parallel to $\mathbf{q}$ and two aligned roughly perpendicular to $\mathbf{q}$. The parallel settings allowed measurement of the angles 10°–60° and 150°–220° while the perpendicular settings allowed measurement of the angles 50°–160°, 230°, and 240° where all angles are measured with respect to $\mathbf{q}$. Within this scheme, 28 correlation data points were measured between 10° and 240° in steps of 10°. Since any geometrical inconsistencies between the two telescope configurations could lead to a false asymmetry in the measured angular correlations, four of these angles (typically 50°, 60°, 150°, and 160°) overlapped in the different settings. A representative goniometer configuration and a telescope cross section are shown schematically in Figs. 2 and 3, respectively.

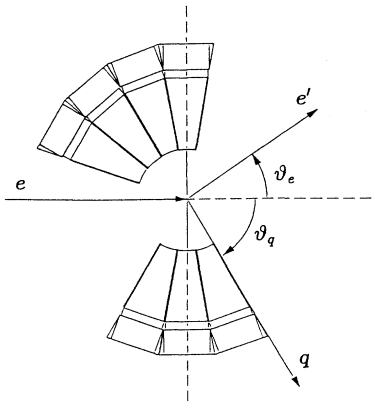

FIG. 2. A representative telescope configuration. The telescopes were mounted on a ring that could be rotated out of the electron scattering plane about $\mathbf{q}$ and rotated in its own plane. This allowed for the measurement of complete angular correlations.

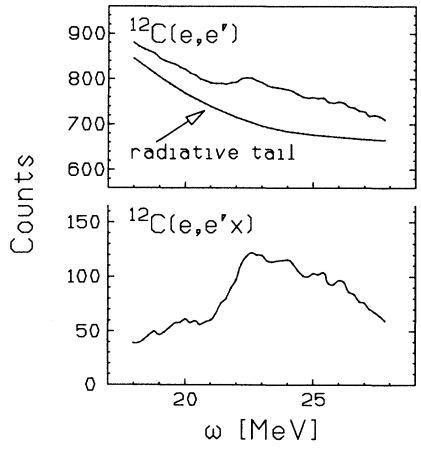

FIG. 4. ^{12}C(e,e') singles spectrum (top) and corresponding ^{12}C$(e,e'x)$ raw coincidence spectrum (bottom) for $q = 0.61$ fm^{-1}. The radiative tail was calculated using the program ALLFIT [18], and the coincidence spectrum is the sum of seven telescopes configured in the parallel goniometer setting.

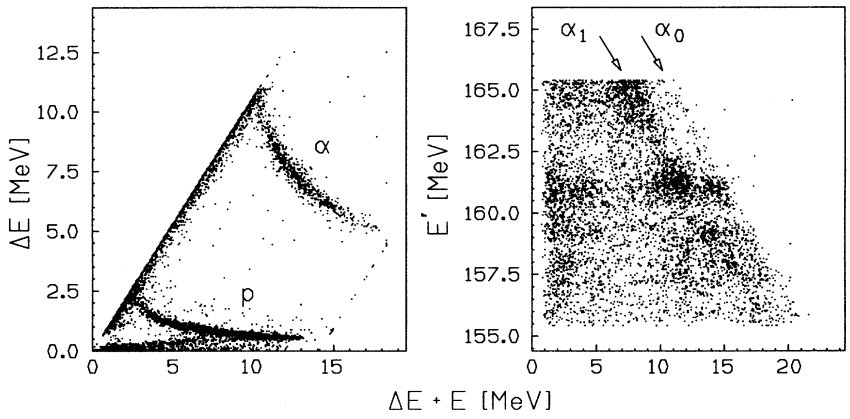

FIG. 5. A typical $^{12}C(e,e'x)$ particle identification (PID) spectrum (left) and scattered electron energy (E') vs particle x kinetic energy spectrum (right). The left spectrum indicates proton (p) and alpha (α) components. The right spectrum, derived by invoking the appropriate α cuts, indicates two final states populating definite kinematically allowed loci (labeled α_0 and α_1). For both spectra, background has not been subtracted. The labels ΔE and $\Delta E + E$ indicate energy deposited in the first and both detectors, respectively.

IV. DATA REDUCTION

To illustrate the power of the coincidence technique, a sample ($q = 0.61$ fm^{-1}) $^{12}C(e,e')$ singles spectrum (top) and corresponding $^{12}C(e,e'x)$ raw coincidence spectrum (bottom) are shown in Fig. 4. Here, the radiative tail was calculated using the program ALLFIT [18], and the coincidence spectrum is the sum of seven telescopes configured in the parallel goniometer setting.

In order to identify the true and accidental coincidence events, cuts were made on the following spectra: (1) one-dimensional TDC spectra, (2) pulse height vs coincidence time distributions, (3) particle identification (PID) spectra which allowed for the separation of the various emission products based on mass and charge, and (4) scattered electron energy (E') vs particle x total kinetic energy ($\Delta E + E$) spectra which allowed for the separation of resolved final state particles for a given particle type. Figure 5 shows typical raw PID (left) and E' vs $\Delta E + E$ (right) spectra for a momentum transfer of 0.61 fm^{-1}

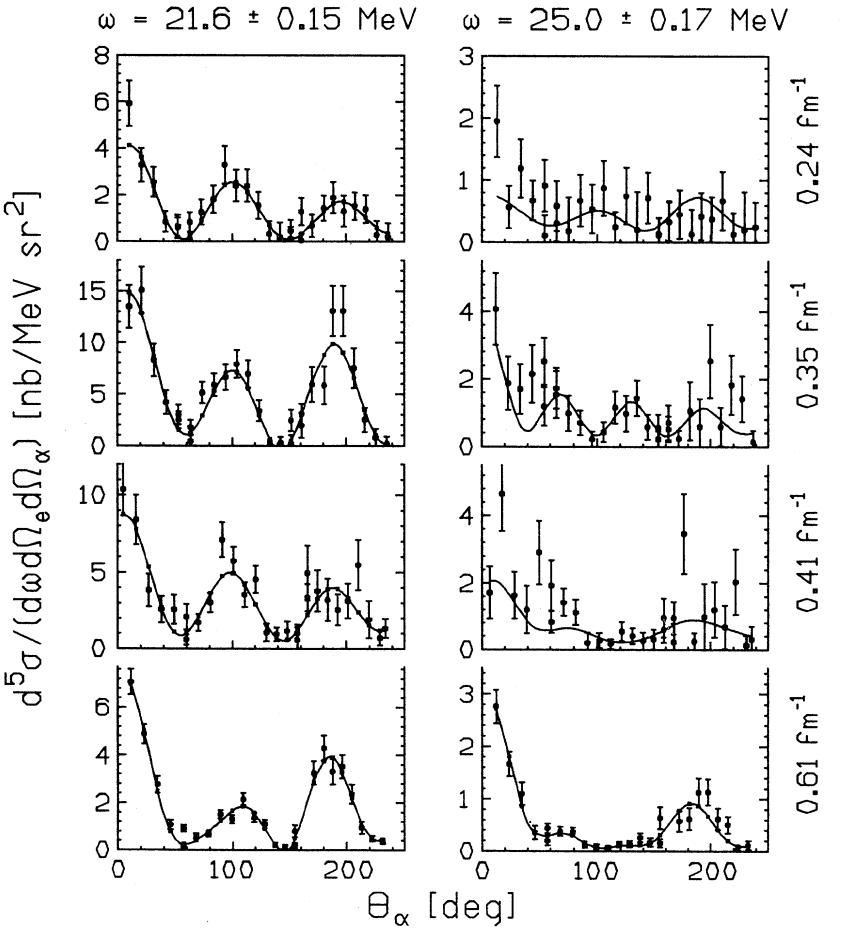

FIG. 6. $^{12}C(e,e'\alpha_0)$ angular correlations for two energy regions for each q point. The curves are Legendre polynomial fits which indicate dominant $E2$.

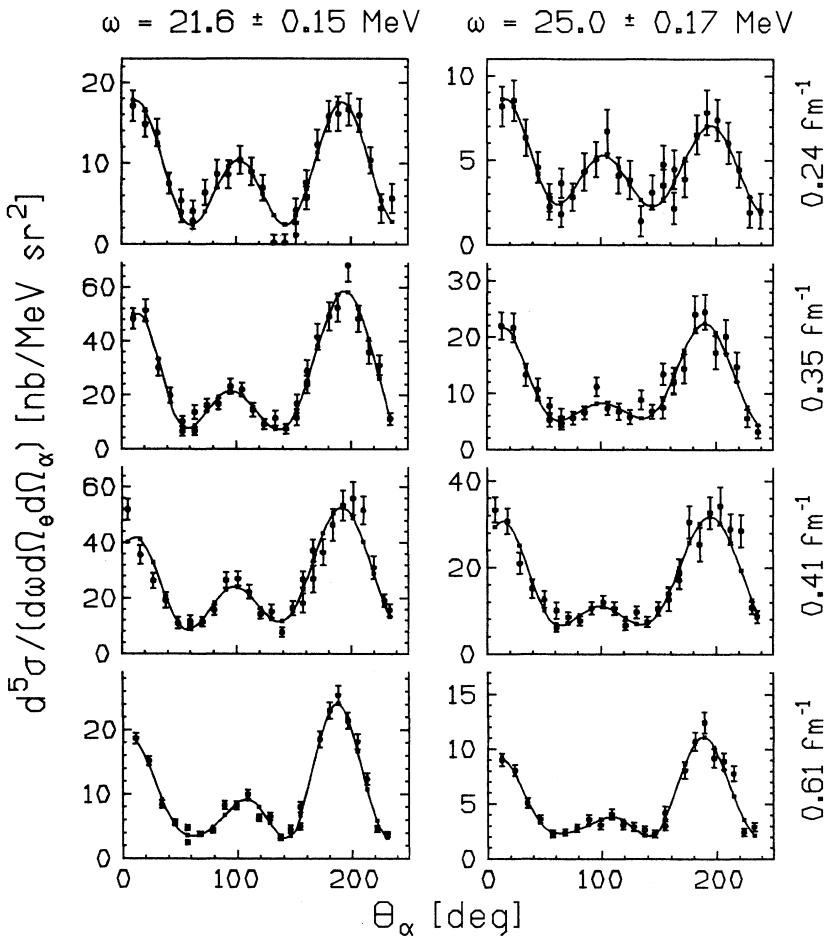

FIG. 7. ^{12}C$(e,e'\alpha_1)$ angular correlations for two energy regions for each q point. The curves are Legendre polynomial fits which indicate dominant $E2$.

and an emission angle of 10°. The latter spectrum was derived by invoking the appropriate α cuts, and background has not yet been subtracted. Separation between the first two final states which populate definite kinematically allowed loci (labeled α_0 and α_1 in Fig. 5) was achieved for all q points and all emission angles.

After cuts were performed, the data were normalized. The normalization was achieved for each q by extracting the proton as well as the α data, normalizing the proton data from our analysis to the same proton data previously analyzed and correctly normalized [19], and then applying the same overall factor to the α data. Each normalization factor included corrections for electronic deadtime, inefficiencies in the electron focal plane, and variations in the spectrometer acceptance.

Finally, cross sections plotted as a function of the center-of-mass (c.m.) α-emission angle were generated for all $\Delta\omega$ and for all q. Figures 6 and 7 show angular correlations for α_0 and α_1 emission for the four-momentum transfer points and for excitation energies of 21.6±0.15 MeV and 25.0 ± 0.17 MeV. The curves come from fits to the Legendre expansion and will be discussed in the next section.

V. DATA ANALYSIS

The correlations were fit to the Legendre expansion [Eq. (7)] and resonance formalism [Eqs. (8)–(12) and the Appendix] via the method of least squares; we included the appropriate Legendre coefficients in the first case, and excitation form factors and angular correlation shape coefficients in the second case as the fit variables. In both cases, this procedure was often rendered intractable by demanding that too many coefficients be determined. It was, therefore, necessary to invoke as many constraints as possible. By simply observing the form of the angular correlations for both α-emission channels one can derive a reasonably accurate picture of how to proceed.

The expectation is that $E2$ radiation is dominant due to the observation that there are relative maxima in most correlations around 0°, 90°, and 180° as shown in Figs. 6 and 7. The asymmetry between the forward-angle and backward-angle cross sections is consistent with interference of this dominant $E2$ multipole with one of opposite parity, namely $E1$, $E3$, or both. The isotropic component observed in some correlations uniquely indicates the presence of $E0$ radiation. Further, magnetic multipoles are forbidden by parity conservation. Finally, for the kinematics chosen, we expect $|C(L)|^2 \gg |T(L)|^2$.

For the Legendre analysis, the condition for a coefficient to be nonvanishing is the same for A_k^0 and A_k^1 and depends on the multipolarity of the radiation and the kinematics. The selection rules lead to the following conditions: for pure radiation of multipolarity L, $k \leq 2L$ and is even; for interfering radiation of multipolarity L

and L', $k \leq L + L'$ and is even (odd) if $L + L'$ is even (odd). For the Legendre fits then, it appeared that coefficients up to order $k = 6$ were sufficient to describe the data since it is unlikely that $L > 3$ will contribute significantly for $q \leq 0.61$ fm^{-1}.

The best Legendre fits to α_0 and α_1 emission were achieved via inclusion of A_0^0–A_6^0, A_2^1, A_4^1, and A_6^1 for a total of 10 coefficients to determine. This choice provided us with sensitivity to multipoles up to $E3$. Fits were attempted with k up to 8, but the coefficients with $k = 7$ and 8 were consistent with zero, thus substantiating our expectation. In all cases, inclusion of odd A_k^1 coefficients resulted in very large errors evaluated for all fit parameters and an unphysical ω dependence for the A_0^0 coefficient. However, given the quadrupole shape of the correlations and the kinematics chosen, we expect the ratios A_k^1/A_0^0 where k is odd to be small.

For the SLRA analysis, the Legendre results as well as Siegert's theorem were used as constraints. This latter constraint, where the longitudinal and transverse amplitudes are related to each other via the continuity equation, $T(L) = -\sqrt{(L+1)/L}(\omega/q)C(L)$, was invoked only for those multipoles which were not expected to dominate the cross section, namely $E1$ and $E3$. Furthermore, in the case of α_0 emission, due to the spin-0 nature of the ^{8}Be-α_0 system, there is a unique outgoing partial wave for each multipole which determines the correlation shape coefficients and eliminates them as variables to the fit. This provided us with a tremendous advantage in accurately extracting the excitation form factors. For interfering multipoles, since there is a phase that remains ambiguous, the best we could do is set limits on these shape coefficients. For this emission channel, the cross section is best described in terms of $E0$, $E2$, and $E3$ radiation, and with Siegert's theorem used to constrain $T3$, only nine coefficients were needed as variables to the fit. The inclusion of $E1$ radiation produced no significant strength for all ω and all q, but larger uncertainties in the other fitted parameters. Therefore, the $E1$ contribution was found to be negligible in this decay channel—a point which will be examined more closely in a later section.

For α_1 emission, however, we could not similarly uniquely identify the contributing partial waves for pure radiation. This meant that our ability to unambiguously determine the contributing multipoles was lost. The most reasonable α_1 results were obtained with the approximation that the $^5G_2$ partial wave for $E2$ radiation and the $^5H_3$ partial wave for $E3$ radiation did not contribute significantly to the cross section. This approximation is reasonable from an angular momentum barrier perspective. Within this constraint, it was concluded that two SLRA fits, neither of which completely characterized the data, were needed. The first fit included $E0$ and its associated shape coefficients as well as $E2$ and $E3$ for a total of 14 fit coefficients, while the second fit included only $E2$ and $E3$ for a total of 11 fit coefficients. We had no way of knowing which parameter set was more reasonable based on the reduced chi-square for the correlations since they were virtually identical in each case. However, in the case where $E0$ radiation was included, the extracted $C(0)$ excitation form factor was an essentially uniform fraction of the total cross section, clearly an upper limit for this strength. $E1$ radiation was not included in any of the α_1 fits based on the fact that such strength was not observed for α_0 emission and the observation that the α_0/α_1 branching ratio is q independent (see Fig. 12). It is useful to note that the same branching ratio for the ^{16}O$(e,e'\alpha)$ reaction was also found to be q independent [20].

An essentially model independent way to extract multipole transition strengths from the SLRA fits, and to compare our results to those of other experiments, is through sum rules. Since this comparison is made at the real photon limit ($q = \omega$), the data were analyzed in such a way that an extrapolation to this limit was readily achieved. Specifically, for all q points, the angular correlations were integrated over α-emission angle and the excitation form factors were integrated over various ranges in ω. In this case, the coincidence cross section becomes

$$\int\int \frac{d^5\sigma}{d\Omega_e d\Omega_\alpha d\omega} d\Omega_\alpha d\omega = \frac{d^2\sigma}{d\Omega_e} = 4\pi\sigma_M |F|^2 \ , \qquad (13)$$

where $|F|^2$ is the total form factor for a given multipole. The reduced transition strengths, $B(EL)$, were extracted by fitting these form factors via the hydrodynamic Tassie model where the transition charge density for $L \geq 1$ is given by $\rho_{\rm tr}(r) \propto r^{L-1}\partial_{\rm g.s.}(r)/\partial r$, while the $L = 0$ "breathing mode" density is given by $\rho_{\rm tr}(r) = 3\rho_{\rm g.s.}(r) - r[\partial_{\rm g.s.}(r)/\partial r]$ according to Satchler [21]. In order to extract these strengths accurately, a distorted wave Born approximation (DWBA) calculation was performed using the code FOUBESFIT [22].

FOUBESFIT generates cross sections for a given transition by performing a phase shift DWBA calculation based on a Fourier-Bessel decomposition of the specified charge density. For ^{12}C, the ground state charge distribution was given in terms of the phenomenological two-parameter Fermi function, $\rho_{\rm g.s.}(r) = \rho_0/(1 + e^{(r-c)/z})$, where c is the half-density radius, z is the skin thickness, and ρ_0 is the central density. The Fourier-Bessel expansion of this density is

$$\rho_{\rm g.s.}(r) = \sum_{\nu=1}^{15} a_\nu j_0(\nu\pi r/R) \quad \text{for } r \leq R \ , \qquad (14)$$

where it is assumed that $\rho_{\rm g.s.}(r) = 0$ for $r > R$. An expansion in 15 parameters and a cutoff radius of $R = 9.0$ fm were sufficient for all fits.

Bringing together this ground state charge density and the model for the transition charge density, the experimentally derived total multipole form factors were fit using the method of least squares by allowing c and $B(EL)$ to vary. The initial parameters used for c and z were 2.56 fm and 0.38 fm, respectively [23].

VI. RESULTS

The Legendre coefficients extracted from the fits are presented in terms of A_0^0, A_k^0/A_0^0, and A_k^1/A_0^0. Dividing the A_k^0 and A_k^1 coefficients by A_0^0 removes the energy

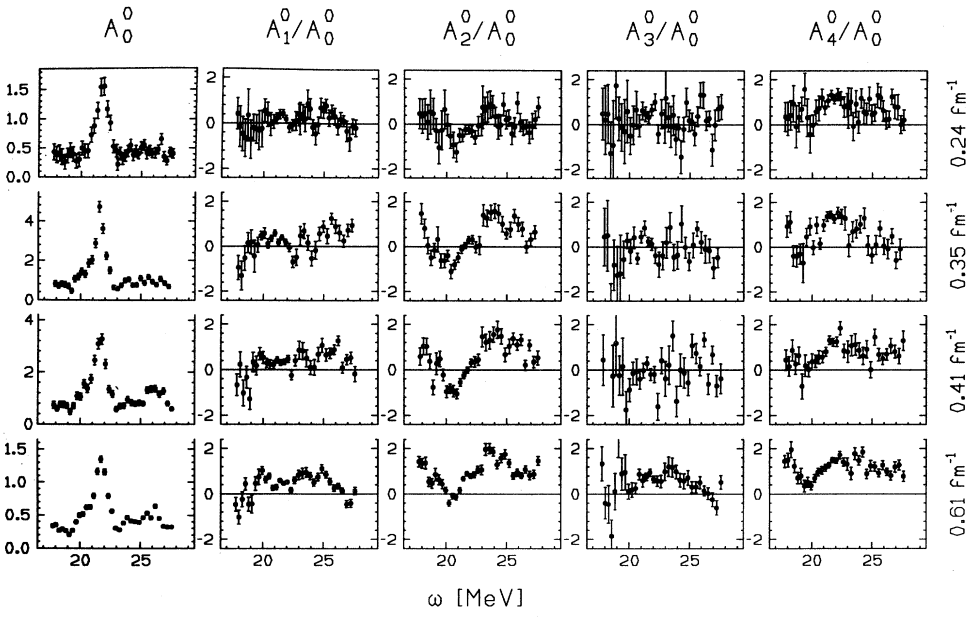

FIG. 8. ^{12}C$(e,e'\alpha_0)$ Legendre fit results as a function of q. The A_0^0 coefficients indicate significant resonant strength centered at 21.6 MeV while the ratios A_4^0/A_0^0 indicate a large $E2$ component.

dependence of the total cross section, leaving a multipolarity "shape" which allows for a more direct comparison between q points.

The α_0 Legendre coefficients are shown in Figs. 8 and 9. The A_0^0 coefficient is dominated by a single resonance which is centered at 21.6 MeV, has a width of ~1.5 MeV, and sits on a relatively monotonic background. The ratio A_6^0/A_0^0, which uniquely indicates the presence of $E3$ radiation, is significant for the highest q point alone, with structure centered at an energy approximately corresponding to that of the resonance. The ratio A_4^0/A_0^0, which indicates $E2$ and/or $E3$ radiation, exhibits structure for all four-momentum transfers at a value of ω centered around the resonance. Given that $E3$ radiation is significant for the highest q point alone, this ratio supports the claim that the α_0-emission cross section is predominantly quadrupole in nature.

The presence of $E1$ radiation must be carefully considered. If isovector (isoscalar) $E1$ strength were present in our data, such strength would be apparent at low (high) momentum transfer due to the q (q^3) dependence of the form factor. The Legendre coefficients that are most sensitive to $E1$ strength are A_1^0, A_2^0, and A_3^0. The first thing to observe is the q dependence of A_2^0/A_0^0. Since this ratio is sensitive to pure radiation, it is useful to look at the angular correlation shape coefficient $a_2(L)$ which is fixed by angular momentum coupling considerations. By using the Appendix, and assuming that the cross section is dominantly longitudinal (which we expect at our kinematics), we can calculate A_2^0/A_0^0 for $E1$, $E2$, and $E3$

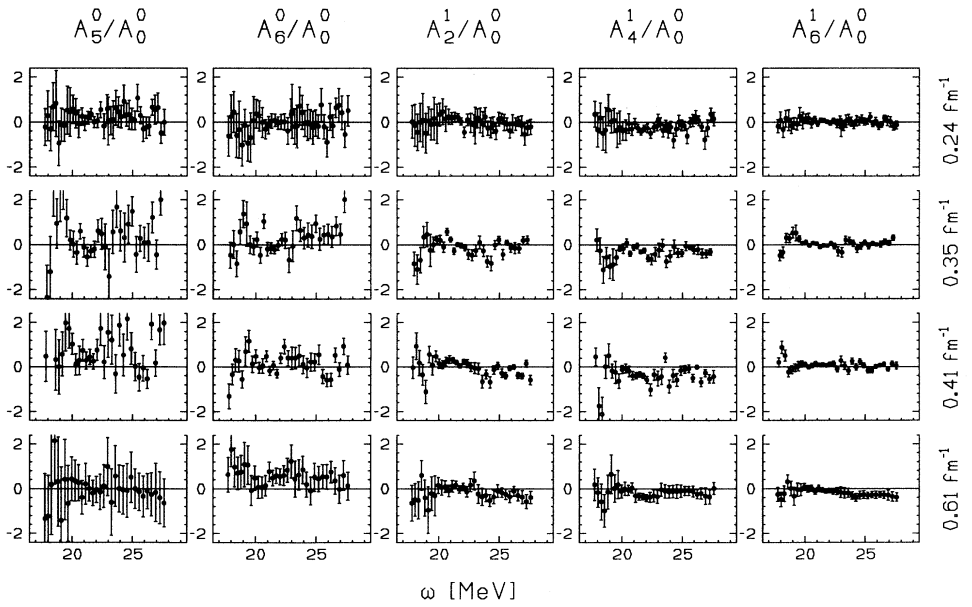

FIG. 9. ^{12}C$(e,e'\alpha_0)$ Legendre fit results as a function of q. The ratio A_6^0/A_0^0 indicates a significant $E3$ contribution for $q = 0.61$ fm^{-1} while the A_k^1/A_0^0 indicate LT contributions.

radiation. This ratio is 2, 10/7, and 4/3 for these multipoles, respectively. That is, the values for $E2$ and $E3$ are essentially identical to each other and significantly different from that of $E1$. Therefore, if isovector (isoscalar) $E1$ strength were present in a significant amount, we would be able to see this at low (high) q. Instead, we observe that A_2^0/A_0^0 is q independent.

Next we observe the q dependence of the ratios A_1^0/A_0^0 and A_3^0/A_0^0 which are sensitive to $E0/E1$, $E0/E3$, $E1/E2$, and $E2/E3$ interference. We have already found that $E3$ radiation is insignificant at $q = 0.24$ fm^{-1} indicating that $E2/E3$ interference cannot be present. What we have left is $E1$ radiation interfering with $E0$ and/or $E2$ radiation. We observe, however, that A_1^0/A_0^0 and A_3^0/A_0^0 are insignificant at low q. This shows that isovector $E1$ strength is not present in our data within statistical uncertainty. At $q = 0.61$ fm^{-1}, we observe that these Legendre ratios have become quite large. We have already found that $E3$ radiation contributes significantly at high q and that A_2^0/A_0^0 is q independent suggesting that isoscalar $E1$ strength is not present. However, due to the limited q range of our data, we must allow for the possibility that this strength exists to some degree. Indeed, isoscalar $E1$ strength has been observed in several light- and medium-weight nuclei [24].

The ratio A_6^1/A_0^0 indicates $E3$ LT interference for the highest q and for large excitation energies, while the ratio A_4^1/A_0^0 indicates that there is (mainly) $E2$ LT interference for all momentum transfers centered around $\omega = 22$ MeV. In both cases, the sign of the interference is consistent with Siegert's theorem. The other Legendre ratios indicate multipole interference at various momentum transfers and energy regions. Unfortunately, we cannot uniquely identify the $E0$ contribution via this method of analysis.

The α_1 Legendre coefficients are shown in Figs. 10 and 11. The A_0^0 coefficient again reveals a well-defined resonance centered at 21.6 MeV with a width of ~ 1.5 MeV. Additionally, there is structure observed at 18.5 and 24.0 MeV. The ratio A_6^0/A_0^0 indicates significant $E3$ strength for the two highest q points, while the ratio A_4^0/A_0^0 indicates that the 21.6 MeV resonance is largely $E2$ in nature with additional quadrupole strength spread out over the full energy range. The remaining A_k^0/A_0^0 ratios indicate multipole interference at various momentum transfers and energy regions while A_4^1/A_0^0 and A_2^1/A_0^0 indicate significant LT contributions. With the Legendre A_0^0 coefficients, and α_0 branch of the total α yield, $\sigma(\alpha_0)/[\sigma(\alpha_0)+\sigma(\alpha_1)]$, can be calculated. Figure 12 illustrates the fact that this ratio is essentially independent of q, indicating that the multipole decomposition of the α_1 channel is the same as that of the α_0 channel. With this observation, the same conclusions about $E1$ strength that were drawn from α_0 emission can be applied to α_1 emission. That is, isovector $E1$ strength is not present within the statistical uncertainty of our data and isoscalar $E1$ strength may be present to some degree at high q.

The best SLRA fits to α_0 emission are shown in Fig. 13. As expected, the total α_0 cross section exhibits the same structure as the Legendre A_0^0 coefficient for all momentum transfers and the $|C(2)|^2$ component of the cross section is dominant with resonant strength centered at 21.6 MeV.

The $|C(0)|^2$ excitation form factor for α_0 indicates significant monopole strength for all q's around 21.0 MeV. It is useful to note that localized $E0$ strength has also been identified via the ^{12}C$(e,e'p_0)$ reaction [25] at around 20.5 MeV, and that both of these results are in good agreement with predictions [26]. Identifying the $E0$ strength distribution is particularly interesting. The centroid energy for this multipole is given by [27] $\omega_{E0} = (\hbar^2 K_A/M_n\langle R_A^2\rangle)^{1/2}$, where M_n is the nucleon mass, R_A is the nuclear radius, and K_A is the nuclear compressibility. To date, most of the information on

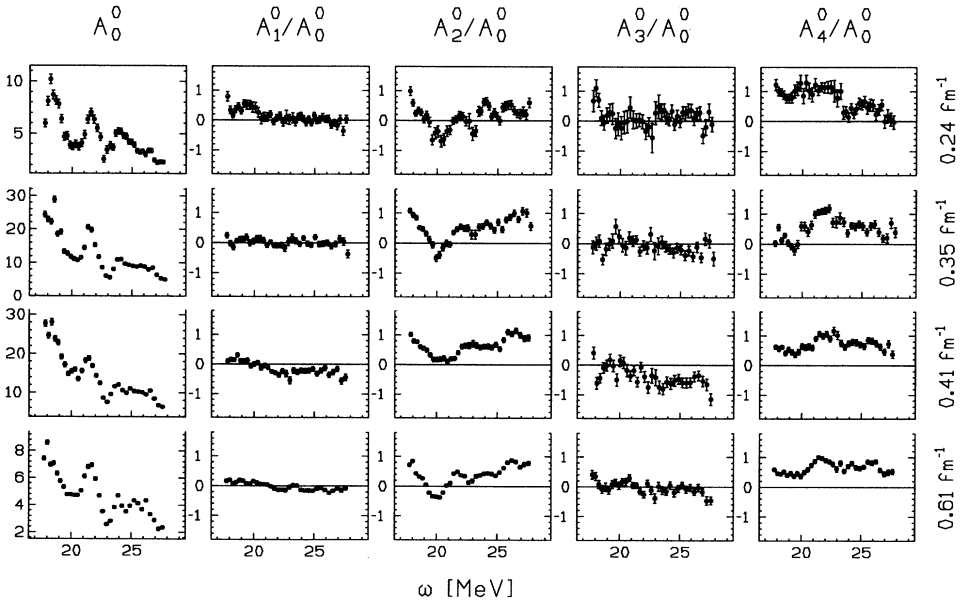

FIG. 10. ^{12}C$(e,e'\alpha_1)$ Legendre fit results as a function of q. The A_0^0 coefficients indicate significant resonant strength centered at 21.6 MeV with additional strength at 18.5 MeV and 24.0 MeV. The ratios A_4^0/A_0^0 indicate a large $E2$ component.

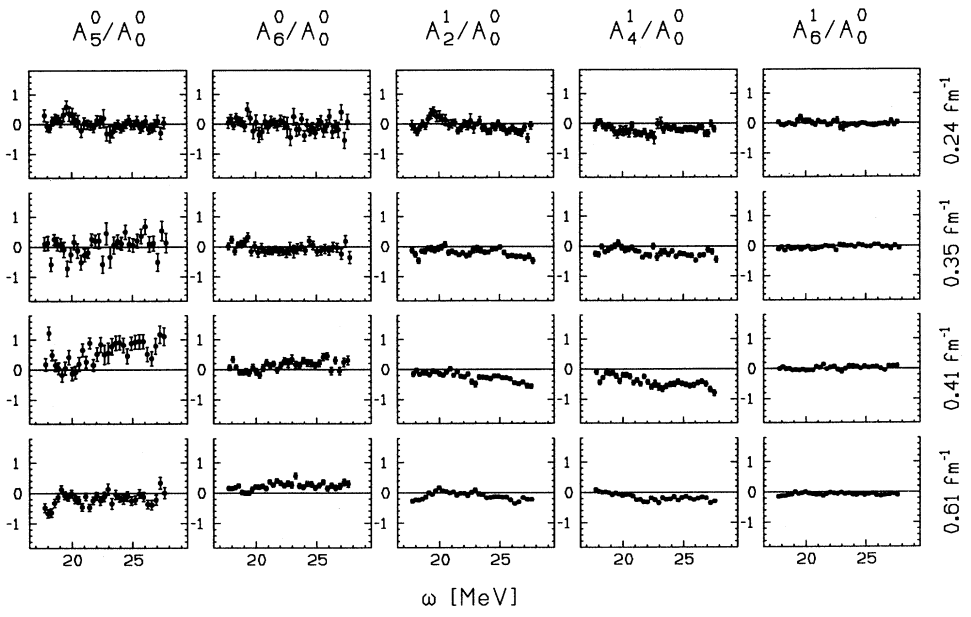

FIG. 11. ^{12}C$(e,e'\alpha_1)$ Legendre fit results as a function of q. The ratio A_6^0/A_0^0 indicates a significant $E3$ contribution at $q = 0.41$ fm^{-1} and $q = 0.61$ fm^{-1} while the A_2^1/A_0^0 and A_4^1/A_0^0 indicate LT contributions.

this multipole (and K_A) comes from small angle inelastic hadron scattering on medium and heavy nuclei [28]. Indeed, the p_0 and α_0 measurements represent the first experimental identification of the continuum monopole distribution in ^{12}C via electron scattering. The $|C(3)|^2$ excitation form factor indicates that the octupole strength is small and fragmented for the three lowest data points, but at $q = 0.61$ fm^{-1} this multipole approaches $\sim 37\%$ of the corresponding $|C2|^2$ strength. Here, as in the Legendre results, this octupole strength peaks at the same excitation energy as for the quadrupole strength.

Since the best SLRA fit results to the α_1 data are those in which only $E2$ and $E3$ contributions as well their interferences were included, only these results are shown in Fig. 14. As expected, the total α_1 cross section reveals the same features as the Legendre A_0^0 coefficient for all momentum transfers. Examination of the squares of the longitudinal excitation form factors indicates dominant quadrupole strength centered at 21.6 MeV. Since we have not included monopole strength in this fit, the $E2$ strength here is an upper limit. The octupole excitation form factor shows some structure around 21.6 MeV for all data points and significant resonant structure at this energy for the highest q.

For both formalisms and both emission particles, the reduced chi-square for all excitation energies was between 1.2–2.5. This, and the similarity between the extracted A_0^0 coefficients and total cross sections, provide confidence in these results.

Table II includes the DWBA transition charge density parameters, multipole transition strengths, and sum rule percentages for α_0 emission and for two energy regions. The first energy region encompasses the 21.6 MeV resonance while the second energy region encompasses the full measured range. We see that for each multipolarity, the fitted value of c is consistent for both energy regions. For the $E0$ form factors, c is consistent with the ground state value while for the $E2$ ($E3$) form factor, c is nominally $1.7c_{\text{g.s.}}$ ($1.5c_{\text{g.s.}}$) for the small energy bin. The expressions used for the multipole transition strengths are related to the excitation form factors and are given by $B(EL) = [(2L+1)!!/q^2]^2|C(L)|^2$ for $L \geq 1$, and $B(E0) = [4\pi \cdot 36/q^2]|C(0)|^2$ for $L = 0$.

Using the following expressions for the electric isoscalar

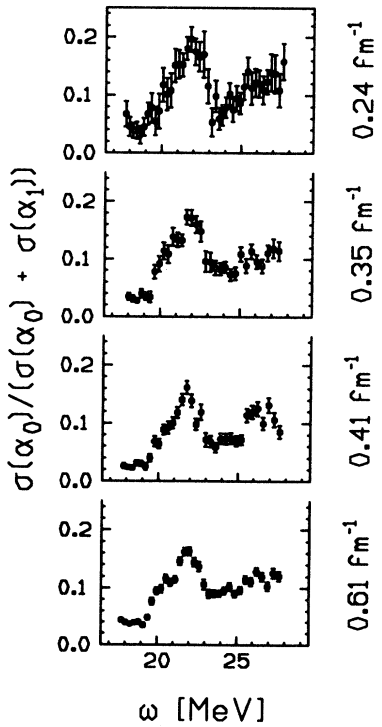

FIG. 12. The fraction of ^{12}C$(e,e'\alpha)$ into the ^{12}C$(e,e'\alpha_0)$ channel as a function of q. The q independence of this ratio validates our multipole decomposition via the SLRA of Kleppinger and Walecka [13].

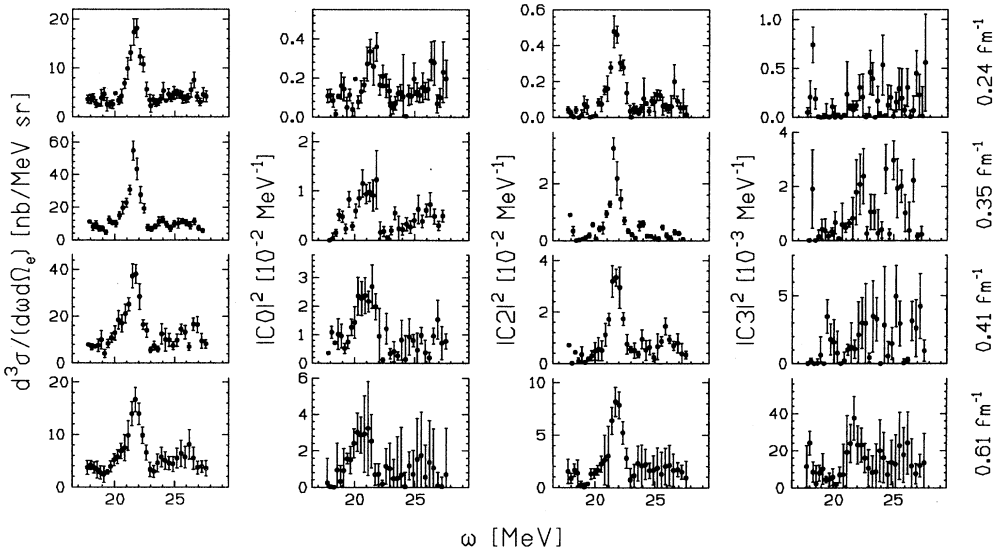

FIG. 13. ^{12}C$(e,e'\alpha_0)$ SLRA fit results as a function of q. The total cross sections indicate significant resonant strength centered at 21.6 MeV. The $C(0)$ and $C(2)$ longitudinal excitation form factors indicate resonant strength for all q's. $C(3)$ strength is observed only for $q = 0.61$ fm^{-1}.

sum rules

$$S(E0, T=0) = 2\frac{\hbar^2 Z^2}{M_p A}\langle r^2\rangle \ , \tag{15}$$

$$S(EL, T=0) = \frac{L(2L+1)^2}{8\pi}\frac{\hbar^2 Z^2}{M_p A}\langle r^{2L-2}\rangle \quad \text{for } L \geq 2 \ , \tag{16}$$

where M_p is the proton mass and $\langle r^2\rangle$ is the mean-squared charge radius of ^{12}C, we find that only a small fraction of the sum rule strengths are exhausted for this emission channel. For the monopole contribution, it is this small sum rule fraction that prevents an accurate evaluation of K_A for ^{12}C since we do not know where the rest of this multipole strength exists.

Table III includes the DWBA transition charge density parameters, multipole transition strengths, and sum rule percentages for α_1 emission, for the two fit trials, and for the same two energy regions as for α_0 emission. We see that for each multipolarity, the fitted value of c is again consistent for both energy regions but different for each fit trial. For the first α_1 SLRA fit (top of Table III), the fitted value of c for $E0$ radiation is consistent with that from α_0 emission while the $E2$ and $E3$ values are larger. Fit parameters for $E3$ radiation for the large energy bin could not be accurately deduced due to the scatter in the data points for this form factor. We expect $E0$, $E2$, and $E3$ radiation to describe the α_1 data just as they did the α_0 data although the actual multipole strengths would be under suspicion due to the inability to fix the angular

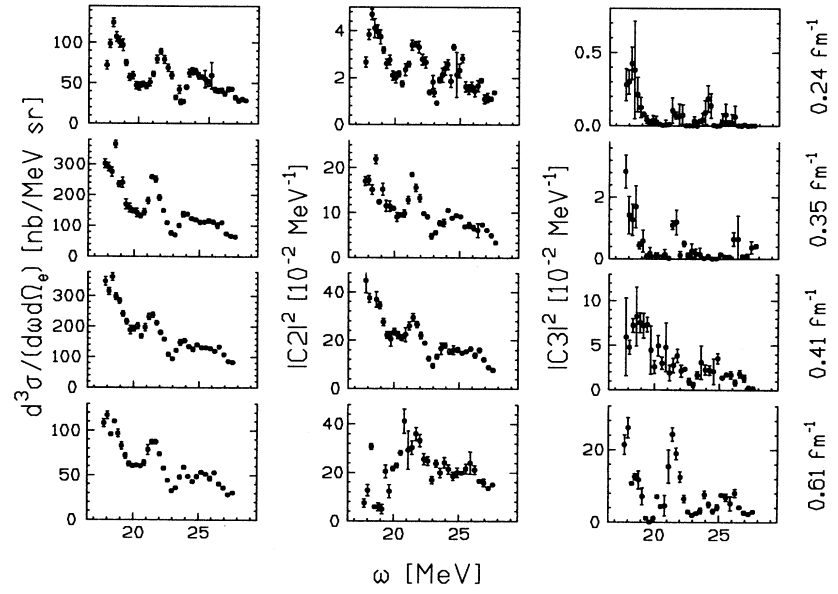

FIG. 14. ^{12}C$(e,e'\alpha_1)$ SLRA fit results as a function of q. The total cross sections indicate significant resonant strength centered at 21.6 MeV with additional strength at 18.5 MeV and 24.0 MeV. It is assumed that the $C(2)$ longitudinal excitation form factors contain $C(0)$ as well. The $C(3)$ resonant strength is $\sim$ 37% of $C(2) + C(0)$ at $q = 0.61$ fm^{-1}.

TABLE II. ^{12}C(e,e',α_0) DWBA Tassie model fit results and sum rule percentages as a function of multipolarity and energy region. The units of $B(EL)$ are e^2fm^4 for $L=0$ and e^2fm^{2L} for $L>0$.

L	ω (MeV)	c (fm)	$B(EL)$	% EWSR
0	20.6–22.6	2.56±0.19	1.10±0.14	1.62±0.21
	18.0–28.0	2.61±0.33	5.12±0.53	7.53±0.78
2	20.6–22.6	4.42±0.43	0.77±0.10	1.09±0.11
	18.0–28.0	4.00±0.27	1.36±0.13	2.00±0.18
3	20.6–22.6	3.9±1.4	23.5±8.7	1.53±0.57
	18.0–28.0	3.6±1.4	78.0±33	5.08±2.1

TABLE III. ^{12}C(e,e',α_1) DWBA Tassie model fit results and sum rule percentages as a function of multipolarity and energy region for two fit trials. The units of $B(EL)$ are e^2fm^4 for $L=0$ and e^2fm^{2L} for $L>0$.

L	ω (MeV)	c(fm)	$B(EL)$	%EWSR
0	20.6–22.6	2.50±0.66	9.7±1.6	14.3±2.4
	18.0–28.0	2.56±0.21	48.9±13.6	71.9±20.1
2	20.6–22.6	4.91±0.50	3.50±0.50	5.14±0.69
	18.0–28.0	5.08±0.51	15.3±3.6	22.4±5.4
3	20.6–22.6	5.64±0.44	178±33	11.6±2.1
	18.0–28.0			
2	20.6–22.6	4.41±0.21	6.96±0.54	10.21±0.80
	18.0–28.0	4.38±0.34	30.6±5.5	44.9±8.1
3	20.6–22.6	3.56±0.38	103±19	6.7±1.4
	18.0–28.0	3.66±0.52	540±39	35.2±2.8

correlation shape coefficients. Instead, the shapes of the $E2$ and $E3$ multipole form factors are different, evidence that that fit does not accurately describe the data. It should be noted that the uncertainties calculated for the $B(EL)$ are a result of the sensitivity of χ^2 to this quantity and are given by the fitting code FOUBESFIT.

For the second α_1 SLRA fit (bottom of Table III), the fitted values of c for $E2$ and $E3$ radiation are nominally the same as those found for α_0 emission, evidence that the data are being described correctly although incompletely. Here, we assume that the fitted $E2$ strength contains $E0$ and $E2$ components—an assumption based on the well-known similarity of the $C(0)$ and $C(2)$ form factors—and that these multipoles exist in the proportion indicated by α_0 emission—an assumption which is supported by the q independence of α_0/α_1 branching ratio as shown in Fig. 12. Given this, we again see that only relatively small fractions of the appropriate sum rules are exhausted.

The α_0 and α_1 form factors and fits for both energy regions are shown in Fig. 15. Included are the $E0$, $E2$, and $E3$ multipole contributions for the α_0 data and the $E0+E2$, and $E3$ multipole contributions for the α_1 data from the second SLRA fit. From this figure, it is apparent that, for both energy bins, the $E2$ and $E3$ multipole form factors have the same q dependence for both α-emission channels as previously indicated in Table III. The $E2$ Tassie model fit suggests that these curves peak at around 0.70 fm^{-1} while the fits for $E3$ radiation continue to rise rapidly, precluding any accurate prediction of a maximum.

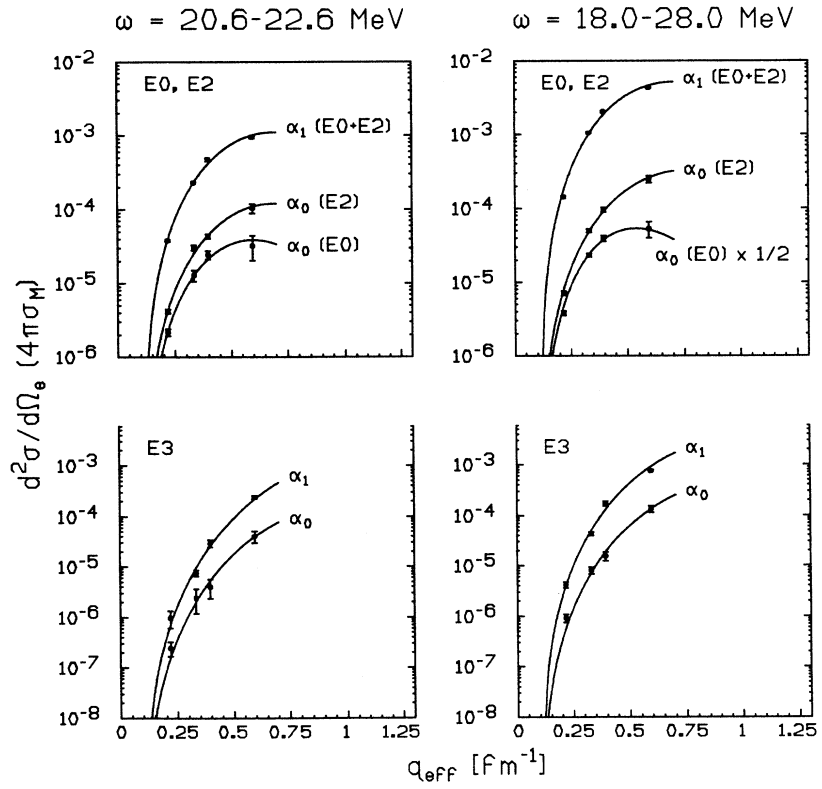

FIG. 15. ^{12}C$(e,e'\alpha_0)$ and ^{12}C$(e,e'\alpha_1)$ total multipole form factors integrated over the 21.6 MeV resonance (left) and the full energy range (right). The curves are Tassie model fits.

VII. COMPARISON WITH OTHER DATA

From our analysis, it is clear that the resonance observed at 21.6 MeV consists of unresolved 2^+ and 3^- isoscalar states. Experiments which have identified this level as 2^+ and $T = 0$ include inclusive α scattering [7], the $(\alpha, \alpha'\alpha)$ reaction [8], and the $(p, p'\alpha)$ reaction [9]. In these cases, the spin and parity were identified by comparing the measured partial angular correlations to a DWBA calculation where the elastic scattering optical-model potential parameters were adjusted for an α particle emitted in the continuum. The cross section in these cases was assumed to be entirely $E2$ in nature even though complete angular correlations were not measured. This assumption is not valid since the detailed fits do not agree with the data over the full angular range, indicating the presence of other multipoles. Experiments which have identified this resonance as 3^- and $T = 0$ include inclusive electron scattering [1] and inelastic proton and α scattering [6]. It is interesting that a state at 21.52 MeV has been identified via p_1, p_2 and α_0 emission after proton capture on ^{11}B [29]. Here, the spin and parity were identified by a fit which produced the best results for all emission particle correlations. Since the α_0 emission width observed for this state was small (~ 0.3 MeV), it was assigned a $T = 1$ nature.

Figure 16 shows the ^{12}C excitation spectrum tagged on α_0 emission (left) and α_1 emission (right) for three different reactions and for $18 \leq \omega \leq 28$ MeV. The top two spectra are the $(e, e'\alpha)$ SLRA results for $q = 0.24$ fm^{-1} and $q = 0.61$ fm^{-1}. Here, the total cross section is represented by the data with error bars while the α_0 (α_1) $E2$ ($E0 + E2$) component is included in histogram form. The lower two spectra are the total cross sections from $(p, p'\alpha)$ and $(\alpha, \alpha'\alpha)$ at momentum transfers of 0.60 and 1.20 fm^{-1}, respectively. In comparing the α_0 data, it is clear that all three reactions show structure around 21.6 MeV. However, the hadron scattering results show significantly more strength outside of the 21.6 MeV peak with additional structure around 19.0 (26.5) MeV for the proton (α) induced reactions. For the α_1 data, all three reactions again show structure around 21.6 MeV. In this case, the proton data closely resemble the electron data while the α data reveal significant additional structure around 26.0 MeV.

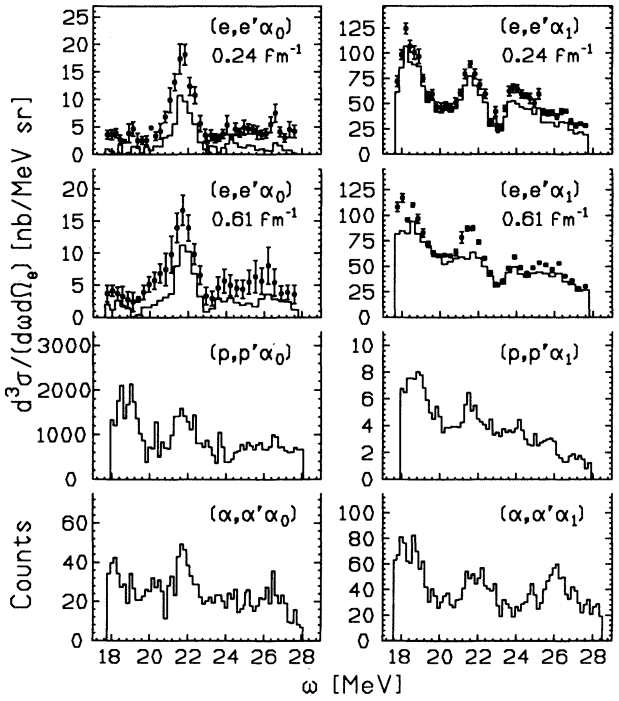

FIG. 16. Comparison of ^{12}C$(e, e'\alpha)$, ^{12}C$(\alpha, \alpha'\alpha)$ [8], and ^{12}C$(p, p'\alpha)$ [9] cross sections. The electron scattering histograms are the $E2$ component of the total cross section.

Table IV summarizes the extracted $E2$ transition strengths and percentages of the isoscalar $E2$ sum rule for α_0 and α_1 emission, for the three reactions, and for comparable energy regions. The errors in the $(e, e'\alpha_0)$ results reflect the statistical uncertainty and the limited q range while the errors in the $(e, e'\alpha_1)$ results are dominated by the systematic uncertainty. This systematic uncertainty is due to the $E0/E2$ ambiguity and was calculated to include the two extremes for $C(0)$. For α scattering, no errors for the sum rule strengths, and no interval for energy integration for the 21.6 MeV resonance, were quoted.

The $(e, e'\alpha_0)$ and $(p, p'\alpha_0)$ $E2$ strengths compare favorably for the 21.6 MeV resonance while the $(e, e'\alpha_1)$ and $(p, p'\alpha_1)$ strengths just agree within the quoted uncertainties. However, the proton induced strengths must be an upper limit since these cross sections were assumed to be entirely $E2$ in nature. Further, since the q for this measurement essentially overlaps with our highest value, we expect the existence of other multipoles. The $(e, e'\alpha_0 + \alpha_1)$ strength is approximately a factor of 5 larger than the $(\alpha, \alpha'\alpha_0 + \alpha_1)$ strength for the 21.6 MeV resonance, and approximately a factor of 4 larger when integrated over an energy bin comparable to our full measured range [8]. The unexpectedly low $(\alpha, \alpha'\alpha)$ strength cannot be explained particularly in light of the fact that no errors were quoted in the literature.

TABLE IV. $E2$ transition and sum rule strengths from ^{12}C(e, e', α) compared to those from ^{12}C$(\alpha, \alpha', \alpha)$ and ^{12}C(p, p', α) [9] as a function of emission particle and energy region. Reference [8] quoted neither the integration region over the 21.6 MeV resonance nor the uncertainties on the estimated $E2$ strength.

Reaction	ω (MeV)	$B(E2)$	% $E2$ EWSR
$(p, p'\alpha_0)$	20.95–22.65		1.4±0.7
	20.95–25.25		2.9±1.4
$(\alpha, \alpha'\alpha_0)$	21.6		0.6
$(e, e'\alpha_0)$	20.6–22.6	0.74±0.07	1.09±0.11
	18.0–28.0	1.36±0.13	2.00±0.18
$(p, p'\alpha_1)$	20.95–22.65		5.0±2.5
	20.95–28.15		15.8±7.9
$(\alpha, \alpha'\alpha_1)$	21.6		1.4
	20.0–30.0		6.4
$(e, e'\alpha_1)$	20.6–22.6	5.60±1.60	8.20±2.3
	18.0–28.0	23.60±4.7	34.7±6.9

VIII. CONCLUSIONS

To summarize, we excited the giant resonance in ^{12}C via inelastic electron scattering and have measured the first complete angular correlations for charged particle emission for this reaction and for four values of momentum transfer ranging from 0.24 fm^{-1} to 0.61 fm^{-1}.

Selecting the α-emission channels provided us with a way to isolate and study the isoscalar resonances. By constructing α-emission angular correlations for all $\Delta\omega$ and fitting these correlations to the Legendre and resonance formalisms, we unambiguously determined the multipole contributions to the total cross section for α_0 emission and have set limits on these contributions for α_1 emission. We found that, in both cases, $E2$ radiation is the strongest contribution, but that $E0$ and $E3$ contributions cannot be ignored. Specifically, for α_0 emission, we found significant $E0$ strength around 21.0 MeV while both emission channels reveal unresolved $E2$ and $E3$ resonant strength at 21.6 MeV.

By constructing total multipole form factors—the first ever for an isoscalar resonance in ^{12}C tagged on α emission—and fitting these form factors within the DWBA and with a transition charge density specified by the Tassie model, we were able to deduce multipole transition strengths. The $E2$ isoscalar sum rule strengths were compared to those deduced from the $(p,p'\alpha)$ and $(\alpha,\alpha'\alpha)$ reactions for both α_0 and α_1 emission and for several energy regions. The result was that our strengths nominally agreed with those from proton scattering and disagreed with those from α scattering. However, for the hadron-induced reactions, the cross section was assumed to be entirely $E2$ in nature and complete angular correlations were not measured implying insensitivity to interfering multipoles.

We found that the α yield from ^{12}C in the resonance region exhausts relatively small fractions of the isoscalar $E0$, $E2$, and $E3$ energy-weighted sum rules indicating, as expected, that these multipole strengths are fragmented for this light nucleus.

ACKNOWLEDGMENTS

This work has been supported, in part, by the Deutsche Forschungsgemeinschaft (SFB 201). The UNH group gratefully acknowledges support by the U.S. Department of Energy (DE-AC02-79ER10330) and the National Science Foundation (INT-821360).

APPENDIX: SLRA CROSS SECTIONS

The coincident cross sections derived within the SLRA for $E0, E1, E2$, and $E3$ radiation as well as their interferences are presented. Here, $F_L(\omega)$ describes the ω dependence of the cross section and BR is the branching ratio for particle x. The other quantities are defined in the text.

$$\frac{d^5\sigma(E0)}{d\Omega_e d\Omega_x d\omega} = \sigma_M F_0(\omega)\mathrm{BR}|C(0)|^2 V_L \ , \tag{A1}$$

$$\frac{d^5\sigma(E1)}{d\Omega_e d\Omega_x d\omega} = \sigma_M F_1(\omega)\mathrm{BR}|C(1)|^2 \Bigg\{ V_L[1 - 2a_2(1)P_2(\cos\vartheta_x)] + V_T\left|\frac{T(1)}{C(1)}\right|^2 [1 + a_2(1)P_2(\cos\vartheta_x)]$$

$$-V_{LT}\frac{T(1)}{C(1)}\sqrt{2}a_2(1)P_2^1(\cos\vartheta_x)\cos\varphi_x + V_{TT}\frac{1}{2}\left|\frac{T(1)}{C(1)}\right|^2 a_2(1)P_2^2(\cos\vartheta_x)\cos 2\varphi_x \Bigg\} \ , \tag{A2}$$

$$\frac{d^5\sigma(E2)}{d\Omega_e d\Omega_x d\omega} = \sigma_M F_2(\omega)\mathrm{BR}|C(2)|^2 \Bigg\{ V_L[1 + 2a_2(2)P_2(\cos\vartheta_x) - \frac{3}{2}a_4(2)P_4(\cos\vartheta_x)]$$

$$+V_T\left|\frac{T(2)}{C(2)}\right|^2 [1 + a_2(2)P_2(\cos\vartheta_x) + a_4(2)P_4(\cos\vartheta_x)]$$

$$+V_{LT}\frac{T(2)}{C(2)}\sqrt{\frac{2}{3}}[a_2(2)P_2^1(\cos\vartheta_x) - \frac{3}{4}a_4(2)P_4^1(\cos\vartheta_x)]\cos\phi_x$$

$$-V_{TT}\frac{1}{2}\left|\frac{T(2)}{C(2)}\right|^2 \left[a_2(2)P_2^2(\cos\vartheta_x) - \frac{1}{6}a_4(2)P_4^2(\cos\vartheta_x)\right]\cos 2\varphi_x \Bigg\} \ , \tag{A3}$$

$$\frac{d^5\sigma(E3)}{d\Omega_e d\Omega_x d\omega} = \sigma_M F_3(\omega)\mathrm{BR}|C(3)|^2\Bigg\{V_L\left[1+\frac{4}{3}a_2(3)P_2(\cos\vartheta_x)+6a_4(3)P_4(\cos\vartheta_x)-\frac{4}{3}a_6(3)P_6(\cos\vartheta_x)\right]$$
$$+V_T\left|\frac{T(3)}{C(3)}\right|^2[1+a_2(3)P_2(\cos\vartheta_x)+a_4(3)P_4(\cos\vartheta_x)+a_6(3)P_6(\cos\vartheta_x)]$$
$$+V_{LT}\frac{T(3)}{C(3)}\frac{2}{3\sqrt{3}}\left[a_2(3)P_2^1(\cos\vartheta_x)+\frac{9}{2}a_4(3)P_4^1(\cos\vartheta_x)-a_6(3)P_6^1(\cos\vartheta_x)\right]\cos\varphi_x$$
$$-V_{TT}\frac{1}{3}\left|\frac{T(3)}{C(3)}\right|^2\left[a_2(3)P_2^2(\cos\vartheta_x)+a_4(3)P_4^2(\cos\vartheta_x)-\frac{1}{10}a_6(3)P_6^2(\cos\vartheta_x)\right]\cos 2\varphi_x\Bigg\}\,, \tag{A4}$$

$$\frac{d^5\sigma(E0/E1)}{d\Omega_e d\Omega_x d\omega} = \sigma_M\sqrt{F_0(\omega)F_1(\omega)}\mathrm{BR}|C(0)||C(1)|\{V_L 2a_1(0,1)P_1(\cos\vartheta_x)+V_{LT}\frac{T(1)}{C(1)}\sqrt{2}a_1(0,1)P_1^1(\cos\vartheta_x)\cos\varphi_x\}\,, \tag{A5}$$

$$\frac{d^5\sigma(E0/E2)}{d\Omega_e d\Omega_x d\omega} = \sigma_M\sqrt{F_0(\omega)F_2(\omega)}\mathrm{BR}|C(0)||C(2)|\{V_L 2a_2(0,2)P_2(\cos\vartheta_x)+V_{LT}\frac{T(2)}{C(2)}\sqrt{\frac{2}{3}}a_2(0,2)P_2^1(\cos\vartheta_x)\cos\phi_x\}\,, \tag{A6}$$

$$\frac{d^5\sigma(E0/E3)}{d\Omega_e d\Omega_x d\omega} = \sigma_M\sqrt{F_0(\omega)F_3(\omega)}\mathrm{BR}|C(0)||C(3)|\{V_L 2a_3(0,3)P_3(\cos\vartheta_x)+V_{LT}\frac{T(3)}{C(3)}\sqrt{\frac{1}{3}}a_3(0,3)P_3^1(\cos\vartheta_x)\cos\phi_x\}\,, \tag{A7}$$

$$\frac{d^5\sigma(E1/E2)}{d\Omega_e d\Omega_x d\omega} = \sigma_M\sqrt{F_1(\omega)F_2(\omega)}\mathrm{BR}|C(1)||C(2)|\Bigg\{V_L\left[\frac{2}{\sqrt{3}}a_1(1,2)P_1(\cos\vartheta_x)-\sqrt{3}a_3(1,2)P_3(\cos\vartheta_x)\right]$$
$$+V_T\frac{T(1)}{C(1)}\frac{T(2)}{C(2)}[a_1(1,2)P_1(\cos\vartheta_x)+a_3(1,2)P_3(\cos\vartheta_x)]$$
$$+V_{LT}\left[\sqrt{\frac{1}{2}}\left(\frac{T(2)}{C(2)}-\frac{1}{\sqrt{3}}\frac{T(1)}{C(1)}\right)a_1(1,2)P_1^1(\cos\vartheta_x)-\sqrt{\frac{2}{3}}\left(\frac{1}{2}\frac{T(1)}{C(1)}+\sqrt{\frac{1}{3}}\frac{T(2)}{C(2)}\right)a_3(1,2)P_3^1(\cos\vartheta_x)\right]$$
$$\times\cos\varphi_x+V_{TT}\frac{1}{6}\frac{T(1)}{C(1)}\frac{T(2)}{C(2)}a_3(1,2)P_3^2(\cos\vartheta_x)\cos 2\varphi_x\Bigg\}\,, \tag{A8}$$

$$\frac{d^5\sigma(E1/E3)}{d\Omega_e d\Omega_x d\omega} = \sigma_M\sqrt{F_1(\omega)F_3(\omega)}\mathrm{BR}|C(1)||C(3)|\Bigg\{V_L\left[\sqrt{\frac{3}{2}}a_2(1,3)P_2(\cos\vartheta_x)-2\sqrt{\frac{2}{3}}a_4(1,3)P_4(\cos\vartheta_x)\right]$$
$$+V_T\frac{T(1)}{C(1)}\frac{T(3)}{C(3)}[a_2(1,3)P_2(\cos\vartheta_x)+a_4(1,3)P_4(\cos\vartheta_x)]$$
$$-V_{LT}\left[\sqrt{\frac{1}{3}}\left(\frac{1}{2}\frac{T(1)}{C(1)}-\sqrt{\frac{2}{3}}\frac{T(3)}{C(3)}a_2(1,3)P_2^1(\cos\vartheta_x)\right.\right.$$
$$\left.\left.+\frac{1}{2}\left(\sqrt{\frac{1}{3}}\frac{T(1)}{C(1)}+\sqrt{\frac{1}{2}}\frac{T(3)}{C(3)}\right)a_4(1,3)P_4^1(\cos\vartheta_x)\right]\cos\varphi_x\right.$$
$$\left.+V_{TT}\frac{1}{6}\frac{T(1)}{C(1)}\frac{T(3)}{C(3)}\frac{1}{24}[a_2(1,3)P_2^2(\cos\vartheta_x)+a_4(1,3)P_4^2(\cos\vartheta_x)]\cos 2\varphi_x\right\}\,, \tag{A9}$$

$$\frac{d^5\sigma(E2/E3)}{d\Omega_e d\Omega_x d\omega} = \sigma_M \sqrt{F_2(\omega)F_3(\omega)}\mathrm{BR}|C(2)||C(3)|\Bigg\{ V_L\sqrt{2}\Bigg[\frac{3}{4}a_1(2,3)P_1(\cos\vartheta_x) + 2a_3(2,3)P_3(\cos\vartheta_x)$$
$$-a_5(2,3)P_5(\cos\vartheta_x)\Bigg] + V_T\frac{T(2)}{C(2)}\frac{T(3)}{C(3)}[a_1(2,3)P_1(\cos\vartheta_x) + a_3(2,3)P_3(\cos\vartheta_x) + a_5(2,3)P_5(\cos\vartheta_x)]$$
$$+V_{LT}\Bigg[\frac{\sqrt{3}}{4}\left(\sqrt{2}\frac{T(3)}{C(3)} - \frac{T(2)}{C(2)}\right)a_1(2,3)P_1^1(\cos\vartheta_x) + \frac{1}{2}\left(\sqrt{\frac{3}{2}}\frac{T(3)}{C(3)} + \sqrt{\frac{1}{3}}\frac{T(2)}{C(2)}\right)$$
$$\times a_3(2,3)P_3^1(\cos\vartheta_x) - \frac{1}{5}\left(\sqrt{\frac{3}{2}}\frac{T(3)}{C(3)} + \frac{2}{\sqrt{3}}\frac{T(2)}{C(2)}\right)a_5(2,3)P_5^2(\cos\vartheta_x)\Bigg]\cos\varphi_x$$
$$-V_{TT}\frac{1}{4}\frac{T(2)}{C(2)}\frac{T(3)}{C(3)}\left[a_3(2,3)P_3^2(\cos\vartheta_x) - \frac{1}{5}a_5(2,3)P_5^1(\cos\vartheta_x)\right]\cos 2\varphi_x\Bigg\} . \qquad \text{(A10)}$$

[1] A. Yamaguchi, T. Terasawa, K. Nakahara, and Y. Torizuka, Phys. Rev. C **3**, 1750 (1971).

[2] R. G. Allas, S. S. Hanna, Luise Meyer-Shützmeister, and R. E. Segel, Nucl. Phys. **58**, 122 (1964); E. Kerkhove, P. Berkvens, R. Van de Vyver, D. Declerck, D. Ryckbosch, P. Van Otten, H. Ferdinand, and E. Van Camp, Phys. Rev. C **29**, 2061 (1984).

[3] J. R. Calarco *et al.* (in preparation).

[4] W. R. Dodge, E. Hayward, R. G. Leicht, B. H. Patrick, and R. Starr, Phys. Rev. Lett. **44**, 1040 (1980); W. R. Dodge, E. Hayward, R. G. Leicht, M. McCord, and R. Starr, Phys. Rev. C **28**, 8 (1983).

[5] M. Buenerd, C. K. Gelbke, D. L. Hendrie, D. Mahoney, C. Olmer, and D. K. Scott, J. Phys. (Paris) Lett. **38**, L53 (1977).

[6] M. Buenerd, P. Martin, P. De Saintignon, and J. M. Loiseaux, Nucl. Phys. **A286**, 377 (1977).

[7] A. Kiss, C. Mayer-Böricke, M. Rogge, P. Turek, and S. Wiktor, J. Phys. G: Nucl. Phys. **13**, 1067 (1987); K. T. Knöpfle, G. J. Wagner, A. Kiss, M. Rogge, and C. Mayer-Böricke, Phys. Lett. **64B**, 263 (1976).

[8] H. Riedesel, K. T. Knöpfle, H. Breuer, P. Doll, and G. Mairle, Phys. Rev. Lett. **41**, 377 (1978).

[9] G. D'Erasmo, I. Iori, S. Micheletti, and A. Pantaleo, Z. Phys. A **299**, 41 (1981).

[10] A. Faessler, D. J. Millener, P. Paul, and D. Strottman, Nucl. Phys. **A330**, 333 (1979); K. T. Hecht and D. Braunschweig, *ibid.* **A295**, 34 (1978).

[11] D. J. DeAngelis, J. R. Calarco, J. E. Wise, H. J. Emrich, R. Neuhausen, and H. Weyand, Phys. Rev. Lett. **70**, 2872 (1993).

[12] T. de Forest, Jr., Ann. Phys. (N.Y.) **45**, 365 (1967); Nucl. Phys. **A392**, 232 (1983).

[13] W. E. Kleppinger and J. D. Walecka, Ann. Phys. (N.Y.) **146**, 349 (1983).

[14] D. Drechsel and H. Überall, Phys. Rev. **181**, 1383 (1969).

[15] A. S. Raskin and T. W. Donnelly, Ann. Phys. (N.Y.) **191**, 78 (1989).

[16] H. Herminghaus, A. Feder, K. H. Kaiser, W. Mainz, and H. v. d. Schmitt, Nucl. Instrum. Methods **138**, 1 (1976).

[17] H. Ehrenberg *et al.*, Nucl. Instrum. Methods **162**, 161 (1972).

[18] J. J. Kelly, C. E. Hyde-Wright, and F. W. Hersman, ALLFIT computer code (unpublished).

[19] H. G. Weyand, Untersuchung der Anregung und des Zerfalls der Dipolriesenresonanz in dem Kohlenstoffisotop ^{12}C durch $(e,e'p)$-Koinzidenzexperimente, Dissertation, Universität Mainz, 1986 (unpublished).

[20] J. P. Fritsch, H. J. Emrich, A. Grasmück, R. Neuhausen, S. Schardt, N. Zimmermann, J. R. Calarco, and M. Potokar, Phys. Rev. Lett. **68**, 1667 (1992).

[21] G. R. Satchler, Part. Nucl. **5**, 105 (1973).

[22] J. Heisenberg, FOUBESFIT computer code (unpublished).

[23] J. A. Jansen, R. Peederman, and C. de Vries, Nucl. Phys. **A188**, 337 (1972).

[24] H. J. Lu, S. Brandenburg, R. DeLeo, M. N. Harakeh, T. D. Poelhekken, and A. van der Woude, Phys. Rev. C **33**, 1116 (1986); T. D. Poelhekken, S. K. B. Hesmondhalgh, H. J. Hofmann, A. van der Woude, and M. N. Harken, Phys. Lett. B **278**, 423 (1992).

[25] J. R. Calarco, J. Arrudo-Neto, K. A. Griffioen, S. S. Hanna, D. H. H. Hoffman, B. Neyer, K. Weinhard, and M. R. Yearian, Phys. Lett. **146B**, 179 (1984).

[26] Y. Kawazoe and T. Tsukumoto, Phys. Rev. C **13**, 1759 (1976); G. Co' (private communication).

[27] J. P. Blaizot, Phys. Rep. **64**, 171 (1980); J. Treinor, H. Krivine, D. Bohigas, and J. Martorell, Nucl. Phys. **A371**, 253 (1981).

[28] A. van der Woude, in *Electric and Magnetic Giant Resonances in Nuclei*, edited by J. Speth (World Scientific, Singapore, 1991), p. 99.

[29] F. Börchers, H. De Jong, J. Krug, and E. Kuhkmann, Nucl. Phys. **A405**, 141 (1983).